5. Results and discussion

5.1. Electrochemical and contact angle results

5.1.1. Pd-Bi-Te

The variation of the current as a function of potential, obtained by changing the potential linearly with time between – 0.2V (SHE) and 0.3V (SHE) at a scan rate of 1mV/s, is shown in Figure 22. (These current-potential curves were measured in triplicate). A small anodic current is evident in the region > 0V in the absence of the collector and is possibly due to the oxidation of the mineral surface. There is a significant anodic current at potentials > 0.2V (SHE) in the presence of potassium ethyl xantante. Two cathodic peaks appear on the return cathodic sweep. These two peaks are due to the reduction of the products of the anodic oxidation. One of the peaks can reflect to reduction of dixanthogen to xanthate, whilst the other may indicate reduction of metal oxides. The potential for equilibrium between ethyl xanthate (10^{-3} M concentration) and pure diethyl dixanthogen is 0.121V (SHE) (Woods *et al*., 1974); this potential is shown in Figures 22 and 28. The section on the Raman investigation (section 5.2.2.) will shed more light on the nature of the reduction reactions.

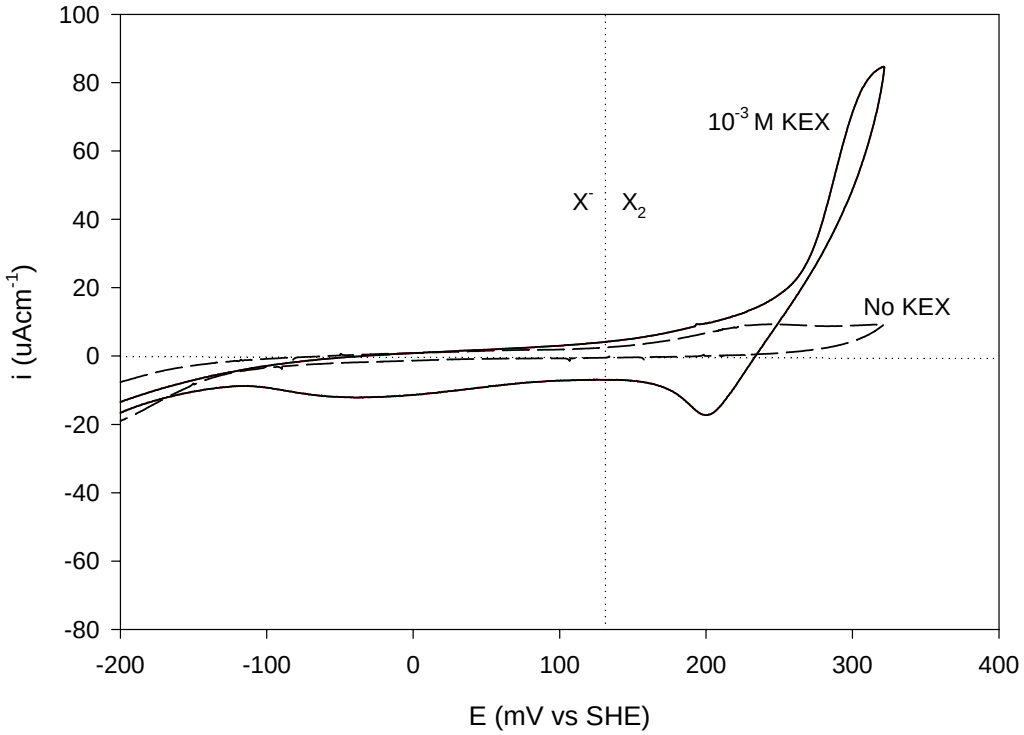

Figure 22: Current-potential curves for a Pd-Bi-Te electrode in a 0.05 M $Na_2B_4O_7$ solution at 25°C in the absence and presence (10^{-3} M KEX) of xanthate collector. Potential sweep carried out at 1mV/s. Starting potential of – 0.2 V (SHE) and positive initial sweep direction.

More detail of the anodic reactions are shown in Figure 23, obtained by changing the potential linearly with time between 0.1 (SHE) and 0.4V (SHE) at a scan rate of 1mV/s. The figure clearly indicates the enhanced anodic activity in the presence of xanthate. In addition to this the figure shows that some oxidation of the mineral occurs in the absence of xanthate, at potentials more positive than 300mV. This anodic current does not originate from adsorption of oxygen only (or from other side reactions). Although anodic current from oxygen adsorption is observed on – for example – pure platinum in this potential range, the charge associated such oxygen adsorption on platinum is in the range 120-400 μC/cm^2 (as found in sulphuric acid (Zolfaghari *et al.*, 2002), potassium hydroxide (Damjanovic *et al.*, 1987) and borate buffer solutions (Woods, 1971), much less than the total anodic charge of 5.8 mC/cm^2 for the mineral in Figure 23.

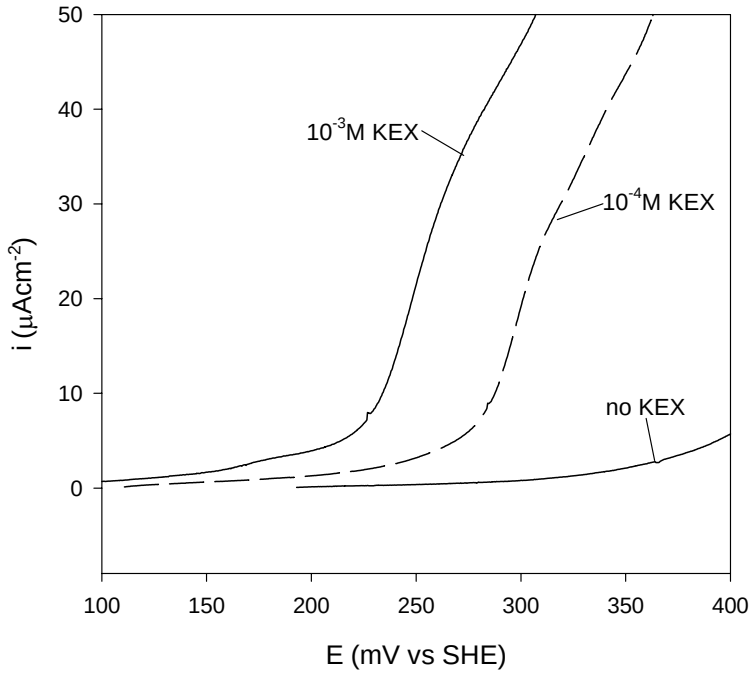

Figure 23: The influence of KEX on the anodic activity for Pd-Bi-Te. Current-potential curves for a Pd-Bi-Te electrode in a 0.05 M $Na_2B_4O_7$ solution at 25°C in the absence and presence of potassium ethyl xanthate. Potential sweep carried out at 1mV/s.

As mentioned earlier, Elvy *et al.* (1994) investigated the incongruent oxidation (in air) of minerals in the Pd-Te-Bi system leading to the formation of layer of tellurium and/or bismuth oxide covering the palladium-rich substrate. It was found that the reactivity of the minerals increased in the order of: PdTe < PdTeBi < PdBi. This is in the same order as the reactivities of Pd, Te and Bi in the pure form. To test whether the same ranking holds in the borate buffer solution, the anodic polarisation behaviour of the pure elements and the Pd-Bi-Te was measured. Figure 24 shows the anodic polarization curves of Bi, Pd, Te and Pd-Bi-Te in a deoxygenated solution containing 0.05 M $Na_2B_4O_7$.

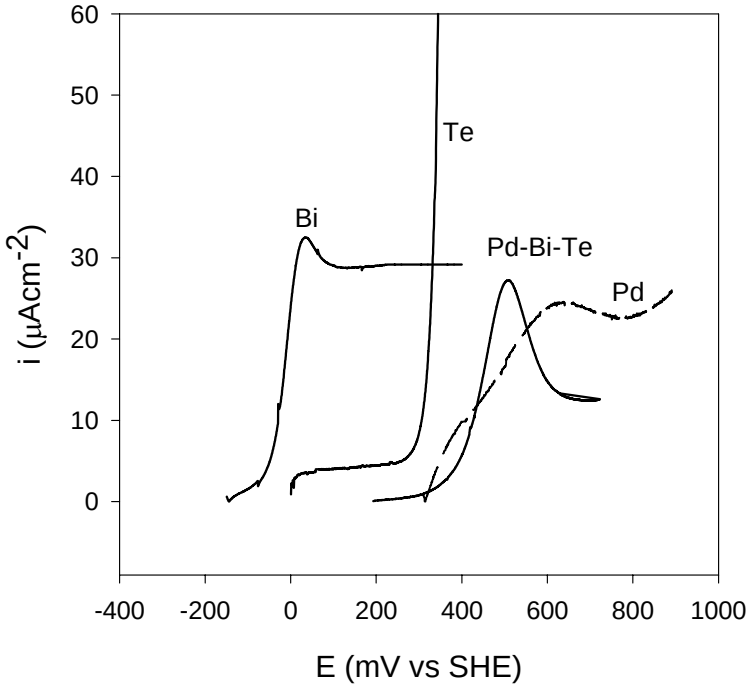

Figure 24: Anodic behaviour of selected metals and alloys in a de-oxygenated solution containing 0.05 M $Na_2B_4O_7$.

Figure 24 clearly shows that Bi is more reactive than Te at potentials lower than 300mV. It is thus expected that minerals containing higher levels of Bi should be more susceptible to oxidation, in agreement with Elvy *et al*. (1994). Although the reactive Bi and Te constitute 66.6 percent (mole basis) of the Pd-Bi-Te mineral, the reactivity of the mineral is much lower than that of the pure constituents. The low palladium activity apparently accounts for the low reactivity of the mineral: as shown in figure 24, the anodic behaviour of michenerite is very similar to that of pure palladium.

In order to investigate the formation of possible surface layers of collector, the Pd-Bi-Te electrode was polarized for 20 minutes at 0.3V (SHE) in a 0.05 M $Na_2B_4O_7$ solution with or without 1 x 10^{-3} M potassium ethyl xanthate, following which impedance measurements were performed. The results of this experiment are shown in Figure 25.

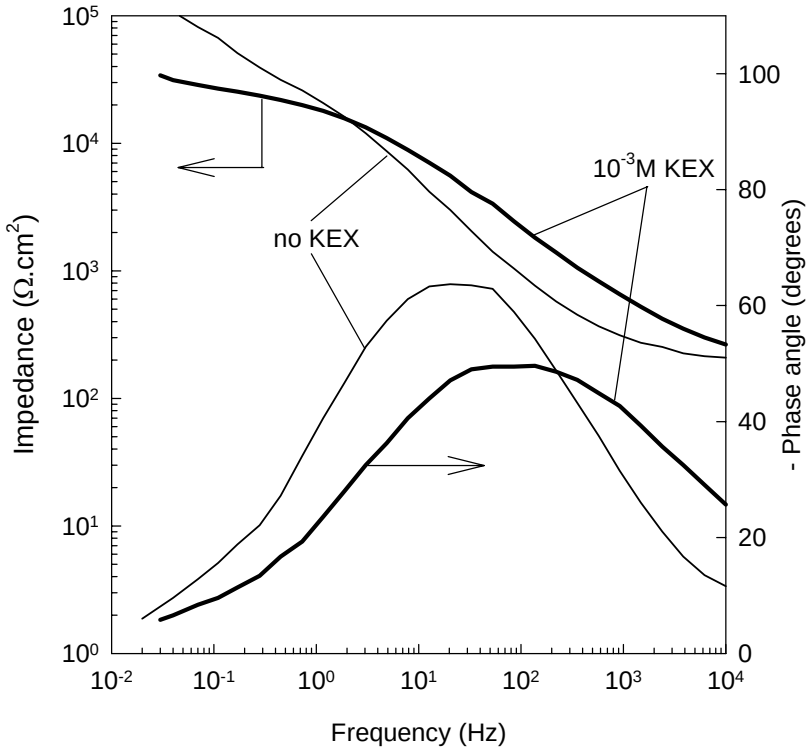

Figure 25: Bode plots for a Pd-Bi-Te electrode after anodic polarisation for 20 min at 0.3V (SHE) in a 0.05 M $Na_2B_4O_7$ solution containing zero and 1 x 10^{-3} M potassium ethyl xanthate.

The contribution of the capacitance value to the impedance is a maximum at intermediate frequencies i.e. where the phase angle is a maximum. The difference in the impedance values (with and without the collector) at intermediate frequencies, see Figure 25, is significant. The fact that a change in the impedance values was observed indicates a change in the capacitance due to the formation of a continuous layer on the surface. The formation of such a layer would tend to decrease the capacitance (see equation 3).

These surface layers can possibly be multi-layers of dixanthogen. Dixanthogen can only form if the mineral surface attains a potential higher than the equilibrium potential of the xanthate-dixanthogen couple. The reversible potential for the oxidation of ethyl xanthate to diethyl dixanthogen is 0.121V (SHE) at a collector concentration of 10^{-3}M KEX (Woods *et al.*, 1974). Efficient cathodic reactions (for

example the reduction of oxygen on the surface of the mineral) would tend to increase the mixed potential. To test whether the potential will be high enough to allow oxidation of xanthate to dixanthogen, cathodic polarisation behaviour and open-circuit potentials were measured. The cathodic polarization diagram showing the reduction of oxygen on the surface, in a borate-only solution, is given in Figure 26.

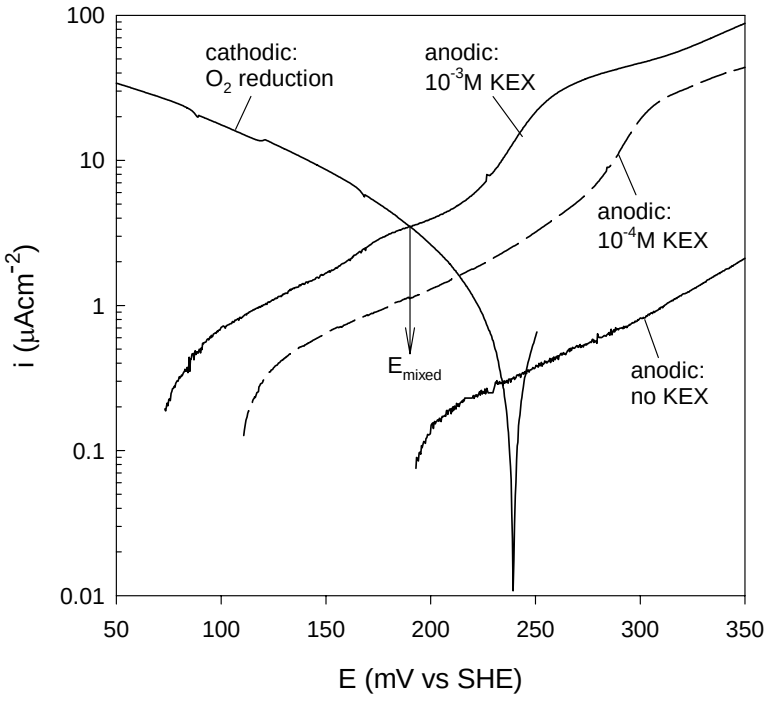

Figure 26: Current-potential curves for a Pd-Bi-Te electrode in a 0.05 M $Na_2B_4O_7$ solution at 25°C in the absence and presence of potassium ethyl xanthate. The anodic polarisation diagrams were measured in deaerated solutions. The cathodic polarisation diagram was constructed in an oxygen-saturated 0.05 M $Na_2B_4O_7$ solution. Potential sweeps carried out at 1mV/s.

The intersection of the cathodic and anodic polarization diagram (for 10^{-3} M KEX) in Figure 26, gives an estimate of the mixed potential (E_{mixed}) for this system. The actual measured mixed potential of the electrode in an oxygen-saturated solution containing 10^{-3} M KEX, is shown in Figure 27.

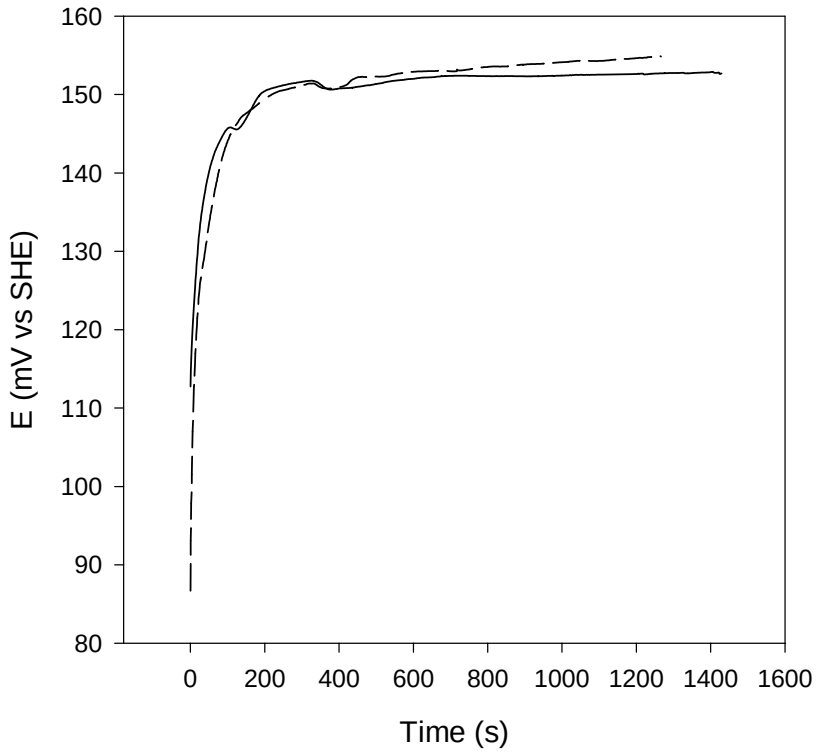

Figure 27: Mixed potential (for two runs) for Pd-Bi-Te in an oxygenated solution containing 10^{-3} M KEX, at a pH value of 9.2.

The mixed potential was measured after freshly preparing the Pd-Bi-Te electrode by grinding and polishing according to the method described in Chapter 4. The borate solution was firstly aerated for 2 hours with oxygen gas whereafter the xanthate was added to obtain a concentration of 10^{-3} M KEX. The electrode was subsequently washed with double distilled water and quickly transferred to the electrochemical cell for measurements. The potential readings commenced the moment the electrode was immersed in the solution (t = 0 s). The true mixed potential (see Figure 27) compares well (difference is less than 30mV) with the value predicted from individual anodic and cathodic polarisation diagrams (see Figure 26). This clearly demonstrates that the mixed potential of the system is higher than the equilibrium potential of the xanthate-dixanthogen couple. It is thus possible for dixanthogen to form on the surface of Pd-Bi-Te.

Contact angle measurements are consistent with the formation of the hydrophobic species (presumed to be dixanthogen) at potentials above the xanthate-dixanthogen

equilibrium potential. Figure 28b shows that, in the presence of ethyl-xanthate, a zero contact angle was observed at those potentials which yielded negligible anodic currents on the voltammograms (for example, 0.1 V in Figure 28a). When the potential was increased to more positive values the contact angle increased strongly. The potential where non-zero contact angles were first observed corresponds well with commencement of xanthate oxidation to dixanthogen. The maximum angle measured was 63 degrees. The contact angle measurements demonstrate that the mineral surface is hydrophobic at high potentials. This hydrophobicity will result in the flotation of the particle if sufficient quantities of the surfactant are present and successful bubble attachment is achieved. This suggests that the poor flotation recovery of the Pd-Bi-Te minerals from flotation feeds cannot be attributed to a lack of interaction between the collector and the mineral surface.

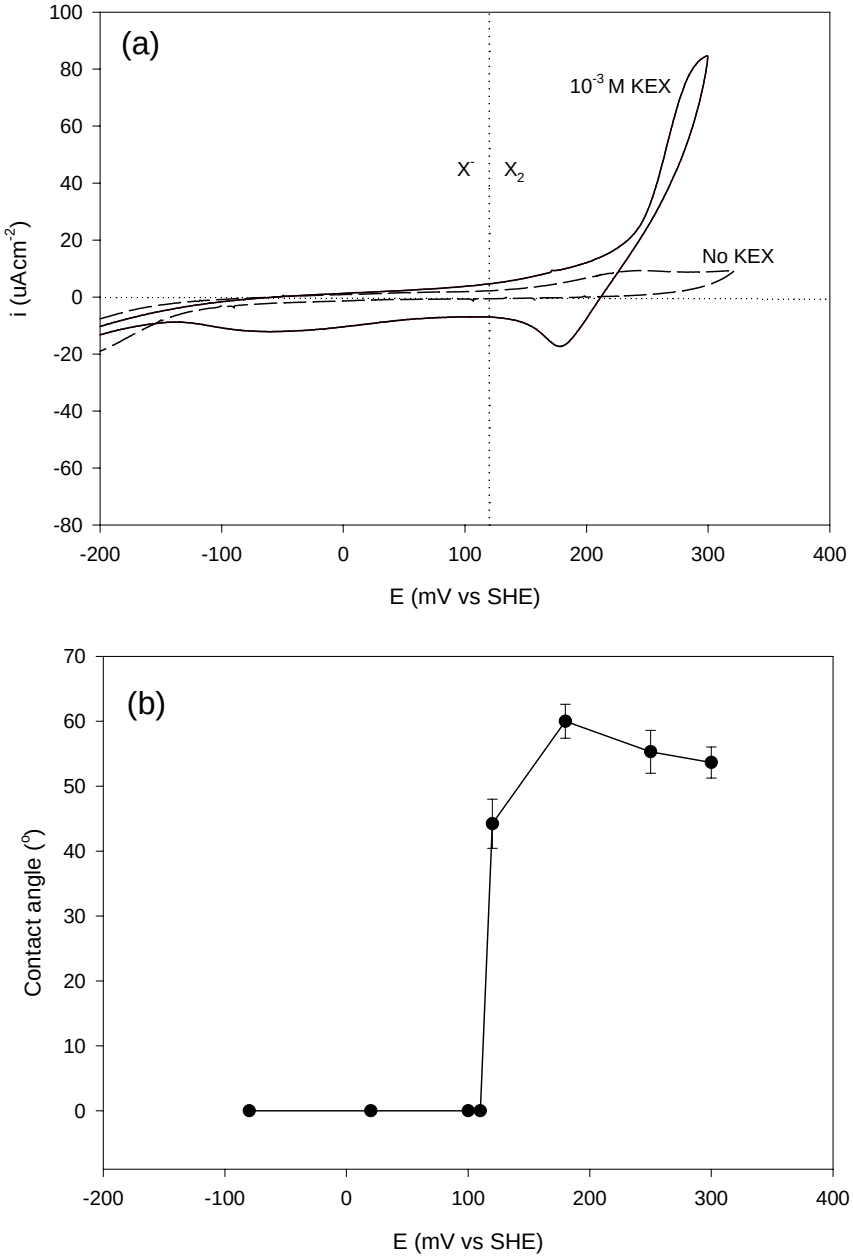

Figure 28: (a) Current-potential curves for a Pd-Bi-Te electrode in a 0.05 M $Na_2B_4O_7$ solution at 25°C in the absence and presence (10^{-3} M KEX) of xanthate collector (data of Figure 22). The equilibrium potential for the oxidation of xanthate to dixanthogen is indicated on the graph. (b) Contact angles for Pd-Bi-Te electrode in a 0.05 M $Na_2B_4O_7$ solution at 25°C in the presence of 10^{-3} M KEX after 300s of polarisation at the relevant potential.

5.1.2. $PtAs_2$

Similar measurements of cathodic and anodic polarisation behaviour and contact angles were performed for sperrylite. Figure 29 shows the cathodic polarisation diagram (measured in oxygen-saturated borate buffer without xanthate), and the anodic polarisation diagram (measured in oxygen-free borate buffer with and without xanthate). Cyclic voltammograms are shown in Figure 30a. Similar to Pd-Bi-Te, the anodic current increases strongly at more positive potentials, in the presence of xanthate. However, for sperrylite the potential where the current starts to increase strongly (0.25 V [SHE]) is significantly more positive than the reversible potential of the xanthate - diethyl dixanthogen equilibrium.

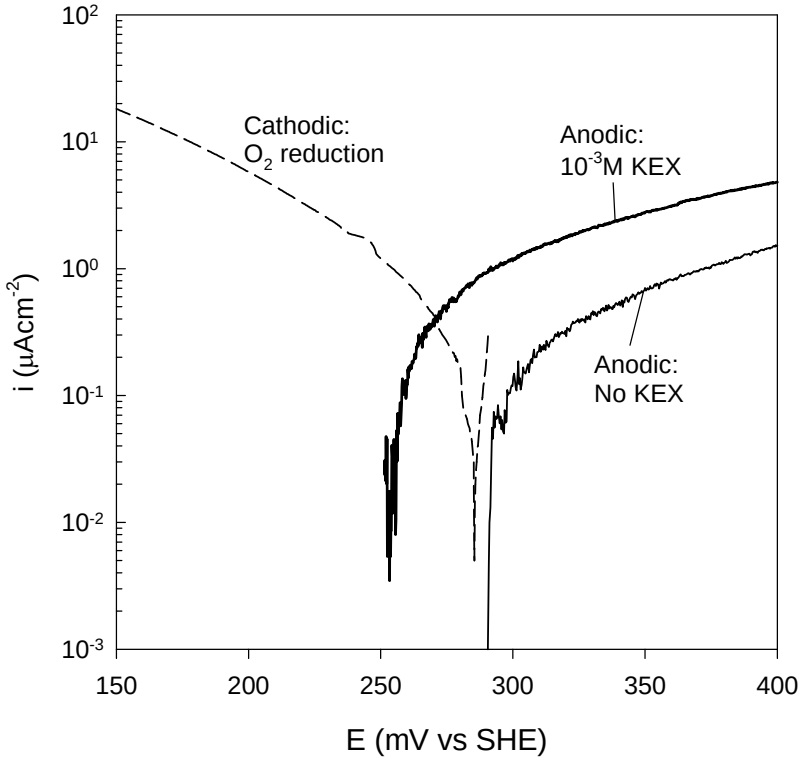

Figure 29: Current-potential curves for a $PtAs_2$ electrode in a 0.05 M $Na_2B_4O_7$ solution at 25°C in the absence and presence of potassium ethyl xanthate. The anodic polarisation diagrams were measured in deaerated solutions. The cathodic polarisation diagram was constructed in an oxygen-saturated 0.05 M $Na_2B_4O_7$ solution. Potential sweeps carried out at 1mV/s.

Figure 30b shows that $PtAs_2$ is hydrophilic at low potentials, with zero contact angles. When the potential was increased to more anodic values the contact angle increased strongly. The maximum angle measured was 54 degrees. The potential where non-zero contact angles were first observed is some 100mV more positive than the xanthate-dixanthogen equilibrium potential, but does correspond to the lowest potential (some 250mV [SHE]) where significant anodic current was measured (see Figures 29 and 30a).

Woods *et al.* (1974) indicated that a maximum contact angle was observed for multilayer surfactant formation, whilst fractional coverages of the surfactant gave rise to smaller angles. The measured contact angles should therefore also depend on the charge transferred during polarisation and not only on the applied potential. This is indeed shown in Figure 31, which shows the dependence of the contact angle on the charge passed (integrated anodic current) in the presence of xanthate (A similar plot cannot be shown for michenerite because currents passed during contact angle measurements were not recorded). Error bands on the charge indicate 95% confidence intervals for at least 2 runs at the same applied potential. Figure 31 shows that the contact angle is independent of the charge transferred for values higher than 50 $mC.cm^{-2}$. Significant contact angles were observed for as low as 8 $mC.cm^{-2}$ charge transferred. The measurement technique used did not allow establishment of the minimum required amount of charge to establish a hydrophobic surface. Woods *et al.* (1974) indicated that a monolayer of dixanthogen is equivalent to a charge of 50 $\mu C.cm^{-2}$. This equivalent charge was calculated based on the assumption that chain length does not affect the packing density of dixanthogen. However Woods *et al.* (1990) showed that efficient flotation recovery occurs with less than a monolayer of collector on the surface.

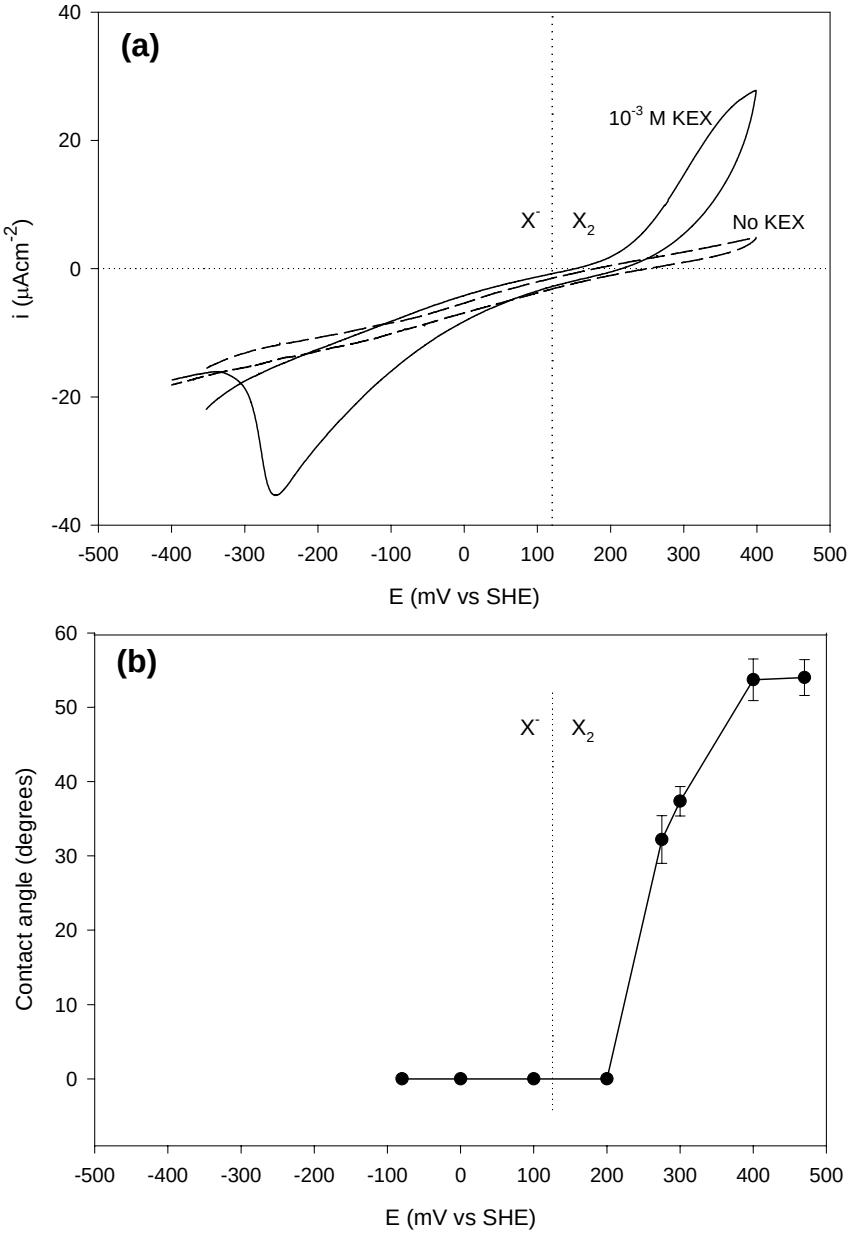

Figure 30: (a) Current-potential curves for a $PtAs_2$ electrode in a 0.05 M borate buffer solution at 25°C in the absence and presence (10^{-3}M KEX) of xanthate collector. Potential sweep carried out at 1mV/s. Starting potential of – 0.4V (SHE) and positive initial sweep direction. The equilibrium potential for the oxidation of xanthate to dixanthogen is indicated on the graph. (b) Contact angles for $PtAs_2$ electrode in a 0.05M $Na_2B_4O_7$ solution at 25°C in the presence of 10^{-3}M KEX after 300s of polarisation at the relevant potential.

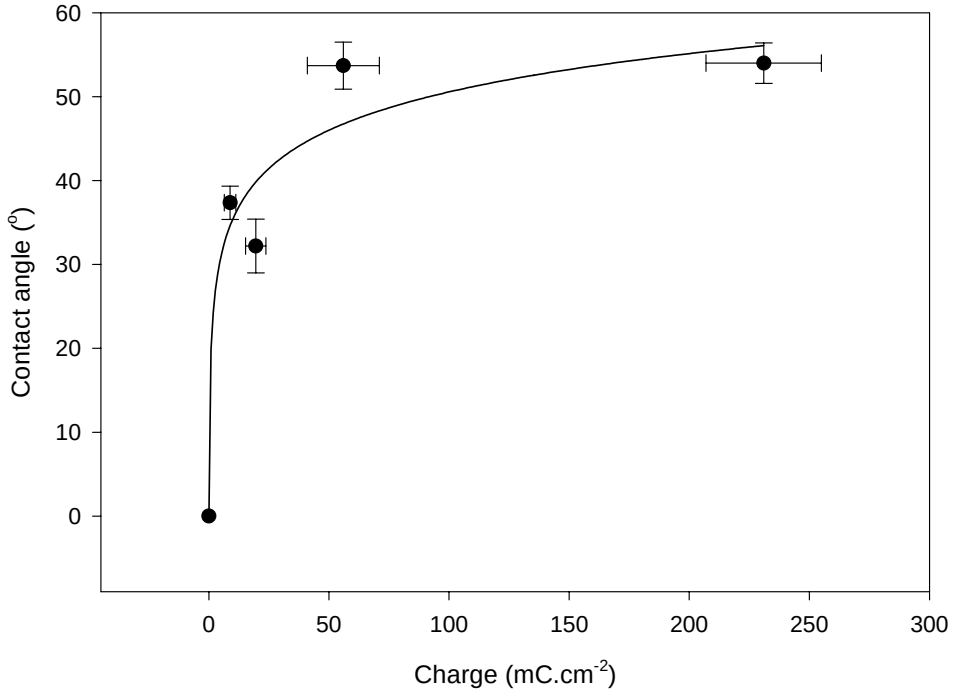

Figure 31: Dependence of contact angle on the charged transferred during anodic polarisation (for the measurements reported in Figure 30) of sperrylite in the presence of 10^{-3}M KEX. Error bands on the charge measured indicate 95% confidence intervals for at least 2 measurements.

5.2. Characteristic peaks in Raman spectra

5.2.1. Collector and oxidised collector

Figure 32 shows the Raman spectra obtained from freshly synthesized potassium ethyl xanthate and diethyl dixanthogen, for reference. The comparative Raman bands of potassium ethyl xanthate and of diethyl dixanthogen are shown in Table 7; the bands are in close agreement with those published by Buckley *et al.* (1997) and Woods *et al.* (1998).

Table 7: The comparative Raman bands of potassium ethyl xanthate and of diethyl dixanthogen. Assignment of the bands of the xanthate compounds was based on the work published by Woods *et al.* (1998).

	Wave number (cm^{-1})			
	Woods *et al* (1998)		This work	
Vibration	KEX (aq)	EX_2 (l)	KEX (aq)	EX_2 (l)
CS_2 antisymmetric stretch	1046	1041	1046	1041
CCOC stretch	864	845	864	844
CS_2 symmetric stretch *trans*	660	695	659	694
CS_2 symmetric stretch *gauche*	615	646	614	646
OCS_2 out of plane *wag*	556	528	-	-
SS stretch	n.a.	498	n.a.	498
COC deformation *gauche*	493	473	493	-
COC deformation *trans*	449	427	448	428
OCC deformation	399	378	401	378

n.a. not applicable

5.2.2. Results of Raman spectroscopy on Pd-Bi-Te

An *in situ* Raman spectrum from a Pd-Bi-Te electrode polarized for 1 hour at 0.3V (SHE) in 0.05 molar sodium tetraborate solution containing 1 x 10^{-3} molar potassium ethyl xanthate is also shown in Figure 32. The 498 cm^{-1} band from the S-S stretching vibration (in dixanthogen) was used to identify dixanthogen on the surface of the minerals (see Table 7). As illustrated by Figure 32, the 498 cm^{-1} Raman band was identified on the Pd-Bi-Te, as were clear bands at 444 and 399 cm^{-1} (slightly shifted from the 448 and 401cm^{-1} bands which are characteristic of xanthate). The small band shift approaches the spectral resolution of the instrument. Nevertheless, a small shift can possibly be attributed to compound formation. It has been shown that the formation of the AuEX radical can be responsible for a shift of 18 cm^{-1} in case of the COC deformation *trans* band (Woods *et al.*, 1998).

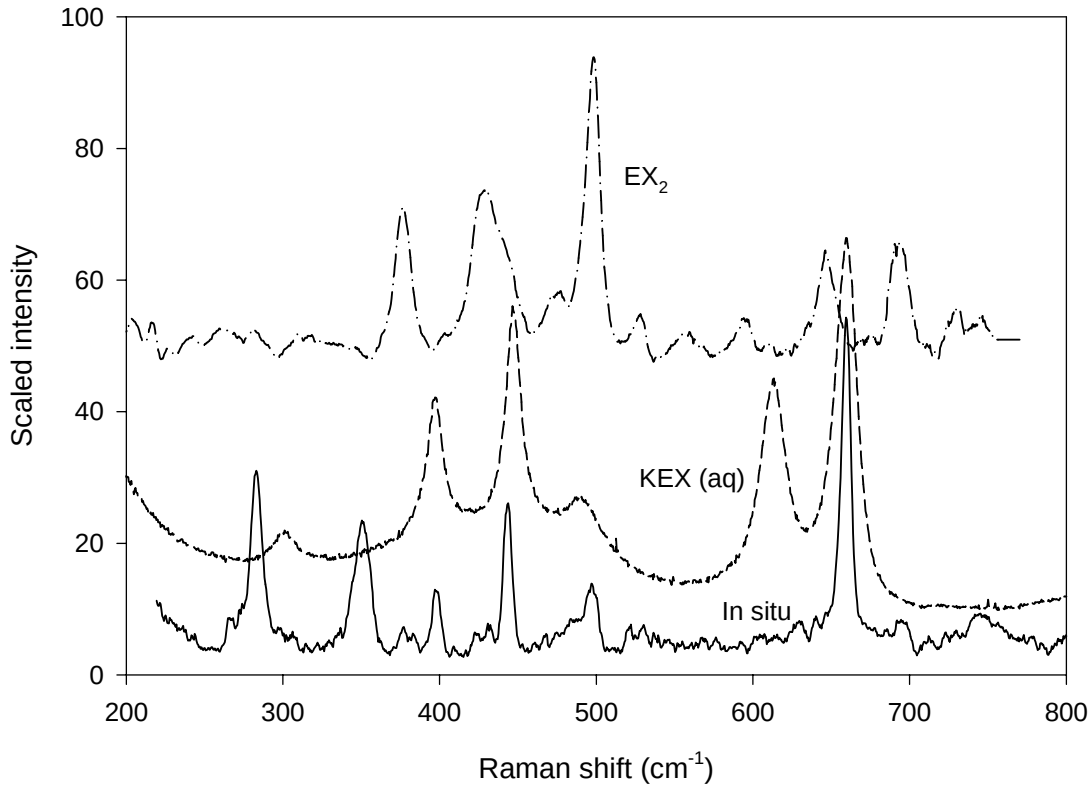

Figure 32: Raman spectra of freshly synthesized potassium ethyl xanthate, diethyl dixanthogen and the *in situ* spectrum of the surface of Pd-Bi-Te anodically polarized in the presence of xanthate for one hour. Laser power rating of 100mW and recording time of 120 seconds.

Extended polarization (at 0.2V [SHE]) of the Pd-Bi-Te electrode for approximately 1 hour in the solution containing 10^{-3}M xanthate caused the formation of visible droplets on the mineral surface. An *in situ* Raman spectrum from these droplets is shown in Figure 33. The spectrum unambiguously shows that ethyl xanthate is oxidized to diethyl dixanthogen on the mineral surface.

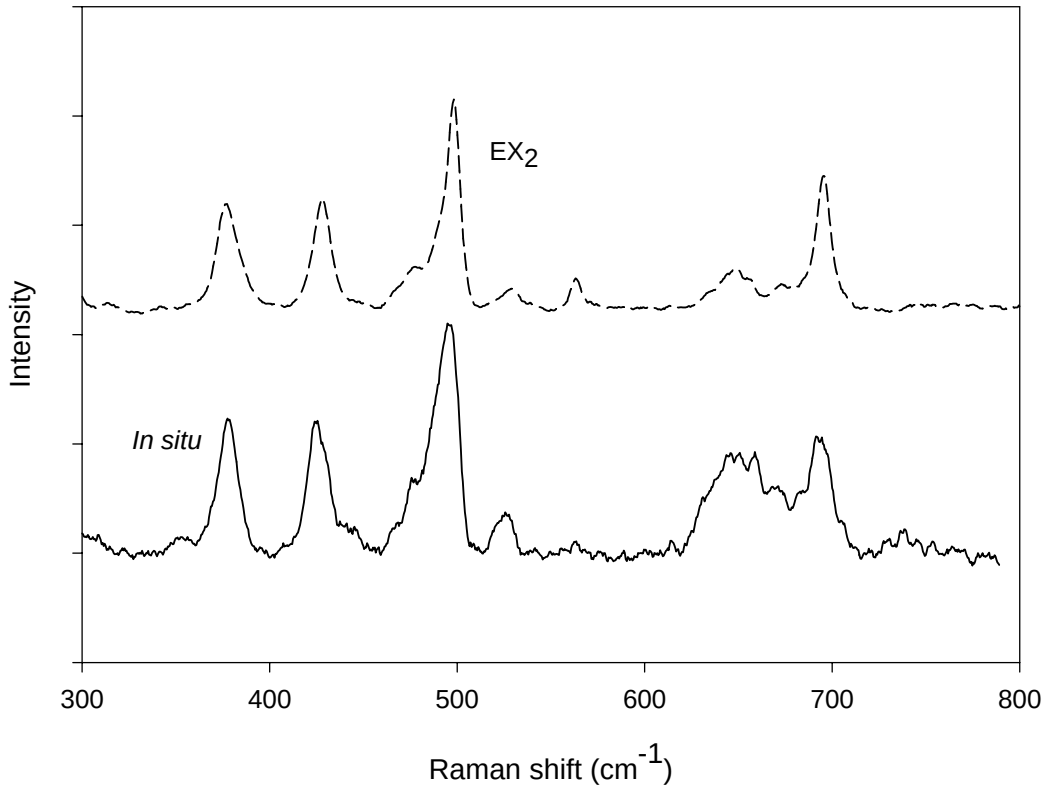

Figure 33: Raman spectra of freshly synthesized diethyl dixanthogen and of droplets on the surface of the Pd-Bi-Te electrode polarized for an hour at 0.2V (SHE) in a 0.05 M $Na_2B_4O_7$ solution containing 1 x 10^{-3} M potassium ethyl xanthate. Laser power rating of 100mW and recording time of 120 seconds.

More detail on the development of the Raman spectrum with polarization time is given in Figure 34, which shows *in situ* Raman spectra from the Pd-Bi-Te electrode polarised at 0.3V (SHE) in a 0.05 M $Na_2B_4O_7$ solution containing 1 x 10^{-3} M potassium ethyl xanthate for different time intervals. Before the start of anodic polarisation, the sample was held at – 0.4V (SHE), where no dixanthogen formation is possible. The spectrum recorded at this potential is labelled with 't=0 s' in Figure 34. It can be seen from Figure 34 that no Raman peak other than the weak and broad 743cm^{-1} band was observed in the spectrum. After anodic polarisation for 120s or longer, xanthate itself is present on the mineral surface: the Raman spectra in Figures 32 and 34 exhibit clear bands at 659 cm^{-1}, which represents a small shift of about 1cm^{-1} from the CS_2 symmetric stretch of xanthate. Notwithstanding this small shift in band

position, the Raman spectra clearly confirm that ethyl xanthate retains its molecular integrity when it adsorbs on the surface of the mineral. Chemisorbed xanthate is the first species to be identified on the mineral surface, with adsorption faster than can be measured by this method (since spectra take 120 seconds to record). Dixanthogen could only be identified on the surface after long exposure times i.e. 1600 seconds in Figure 34. The band that arises from the S-S stretching vibration of dixanthogen at 498cm^{-1} is present in both Figures 32 and 34 (see times from 1600 seconds onwards). This clearly demonstrates that the anodic current recorded in Figure 28a can be attributed to the formation of this compound. Unlike the results for copper and silver Figure 28a does not exhibit any prewave indicative of chemisorption of xanthate (Woods *et al.,* 1998). The absence of the prewave suggests that chemisorption takes place in the same potential region as dixanthogen formation. Woods *et al.* (1998) showed that xanthate chemisorbs at underpotentials on gold, silver and copper. While these results suggest that underpotential deposition does not take place on Pd-Bi-Te, further experiments would be required to resolve this.

The clear bands obtained after even short periods of anodic polarisation indicates that surface enhancement of the Raman bands could have occurred. The phenomenon of surface enhanced Raman scattering (SERS) has been used extensively to characterize surface layers at sub-monolayer coverages (Woods *et al.*, 1998; Buckley *et al.*, 1997; Woods *et al.*, 2000). This phenomenon is surface sensitive and also does not enhance the bands equally; it has been observed on copper, silver and gold (Woods *et al.*, 2000). For the present results - as in the case of gold - the 660 cm^{-1} (xanthate) band shows a greater intensity despite the fact that much more dixanthogen than xanthate should be present on the surface given the relative large overpotential (0.18V) applied. However the anodic oxidation of ethyl xanthate on gold occurs before the formation of the metal xanthate resulting in a potential region (between – 0.057 V and –0.035V) where only dixanthogen is formed on the surface. An *in situ* SERS spectrum taken at a potential within this region showed the presence of a chemisorbed monolayer and dixanthogen (Woods *et al.*, 1998). The hypothesis states that only a monolayer of xanthate is deposited on the mineral with multi-layers of dixanthogen depositing on top of the xanthate layer (Woods *et al.*, 1998). Sustained anodic polarisation at this potential therefore continues the deposition of the dixanthogen, without increasing xanthate coverage. It is believed that the difference in Raman peak

intensities reflect differences in attachment of the two species to the surface (Woods *et al*, 1998). It is postulated that the covalent chemisorbed xanthate gives more signal enhancement than the covalently-bonded dixanthogen. Palladium, however, shows only a small enhancement factor (SERS does occur with palladium under very specific conditions which was probably not the case in this study [Zhong-Qun *et al.*, 2002]) compared to the copper, silver and gold and the presence of a xanthate peak at 660 cm^{-1} should not only be attributed to the formation of the monolayer. The formation of bulk metal xanthate is dependant on the reversible potential of the xanthate-metal xanthate equilibrium potential; this is not known for the metals used in the study. For the gold system, however, at extended polarisation at high potentials dixanthogen and gold xanathate are formed (Woods, 1972). It is, therefore, suggested that a metal xanthate, most probably bismuth xanthate is the major interaction product of the collector with Pd-Bi-Te.

Raman spectroscopy performed on pure Bi and Te electrodes polarized at 0.2V (SHE) in a 0.05 M $Na_2B_4O_7$ solution containing 1 x 10^{-3} M potassium ethyl xanthate for 1 hour did indicate the formation of dixanthogen. However, because of the reactivity of both elements under laser illumination, lower laser power had to be used, to the detriment of the response signal.

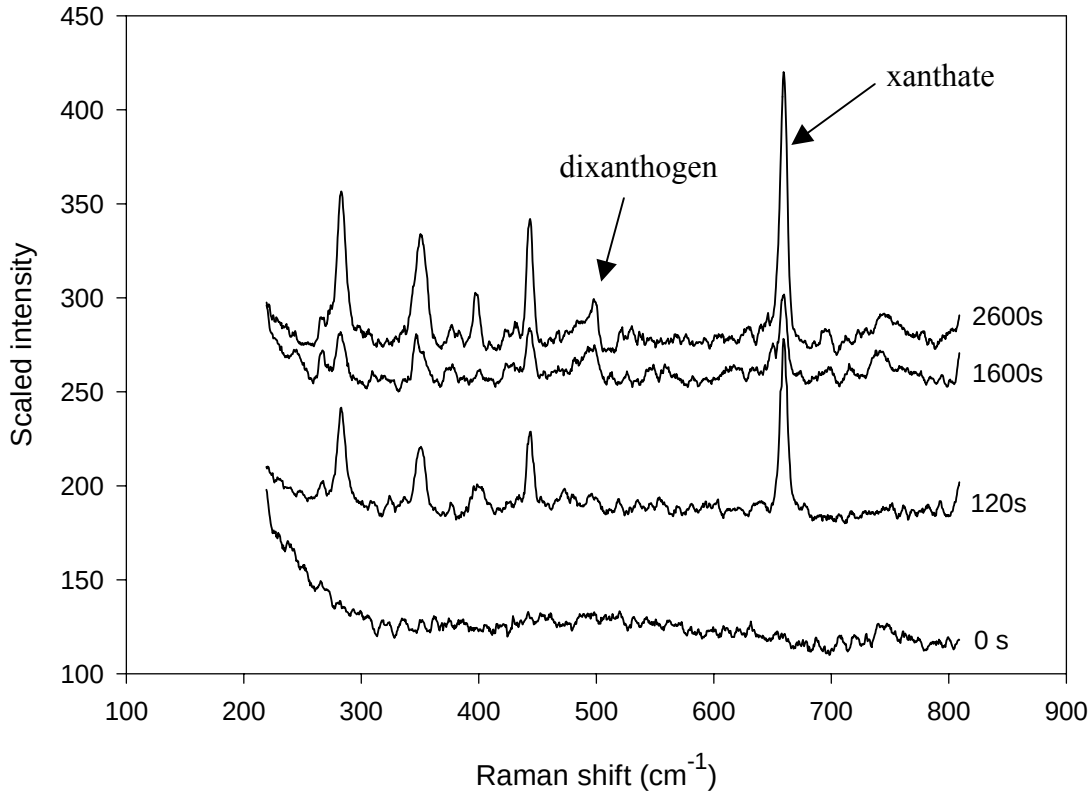

Figure 34: Raman spectra of Pd-Bi-Te electrode polarized for different lengths of time at 0.3 V (SHE) in 0.05M $Na_2B_4O_7$ solution containing 1 x 10^{-3} M potassium ethyl xanthate. Laser power of 100mW and recording time of 120 seconds. Arrows indicate the Raman peaks to be characteristic of xanthate and dixanthogen.

The surface roughness of the mineral plays a vital role in the enhancement of the Raman signal. Figure 35 indicates local variability in the signal strength (which was not the result of differences in focusing; care was taken to focus the beam well in all cases). Despite the variability, general trends can be observed by plotting the ratio of the intensity of the specific band (peak heights) to that of a reference band (see Appendix 11 for spectra and summary of results). The time-lag measurements of which summarised results are shown in Figure 35 were each taken at a new site in close proximity to the previous measurement site. Figure 35 shows the intensity ratio of the 498 cm^{-1} band, corresponding to the S-S stretch or dixanthogen, to that of the reference band. The measurements were grouped in intervals of a 1000s to be able to calculate averages and corresponding standard deviations.

The reference band was the 743 cm^{-1} band. As discussed later the origin of this band is not clear, but the band intensity is relatively insensitive to anodic polarization (see Figure 38 and Table 8).

Table 8: The integrated area of the 743 cm^{-1} band (integrated from 727 cm^{-1} to 760 cm^{-1}) as a function of the anodic polarization time. The Pd-Bi-Te electrode was polarized for different lengths of time at 0.3 V (SHE) in 0.05M $Na_2B_4O_7$ solution containing 1 x 10^{-3} M potassium ethyl xanthate. Laser power of 100mW and recording time of 120 seconds were used.

Polarization time (s)	Area (counts.cm^{-1})
0	197.2
840	188.9
1800	183.6
3000	190.3

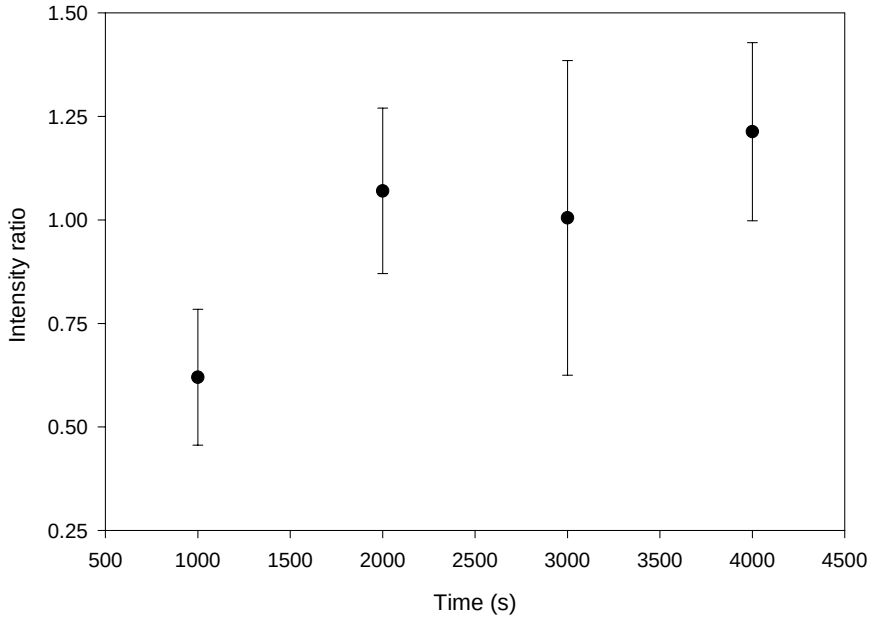

Figure 35: Intensity ratio of 498 cm^{-1} band (indicative of dixanthogen) to that of the 743 cm^{-1} band as a function of the anodic polarization time. Anodic polarization was carried out at 0.3V (SHE) in a 0.05 M $Na_2B_4O_7$ solution containing 1 x 10^{-3} M potassium ethyl xanthate. Error bands indicate 95% confidence intervals for a single run, with around 5 measurements for each 1000s of polarisation time.

These results are in line with the hypothesis that multi-layers of diethyl dixanthogen deposit when the mineral surface is polarized at potentials more anodic than the minimum potential required for dixanthogen formation (Woods *et al.*, 1998). The deposition of the multi-layers over time results in the increase of the amount of dixanthogen as indicated in Figure 35. Figure 36 plots the intensity ratio of the 660 cm^{-1} band (characteristic of xanthate) relative to the 743 cm^{-1} reference band, for the same time intervals as shown in Figure 35. While rather scattered, these results show a constant xanthate peak height (irrespective the presence of xanthate in the form of the chemisorbed layer or the metal xanthate).

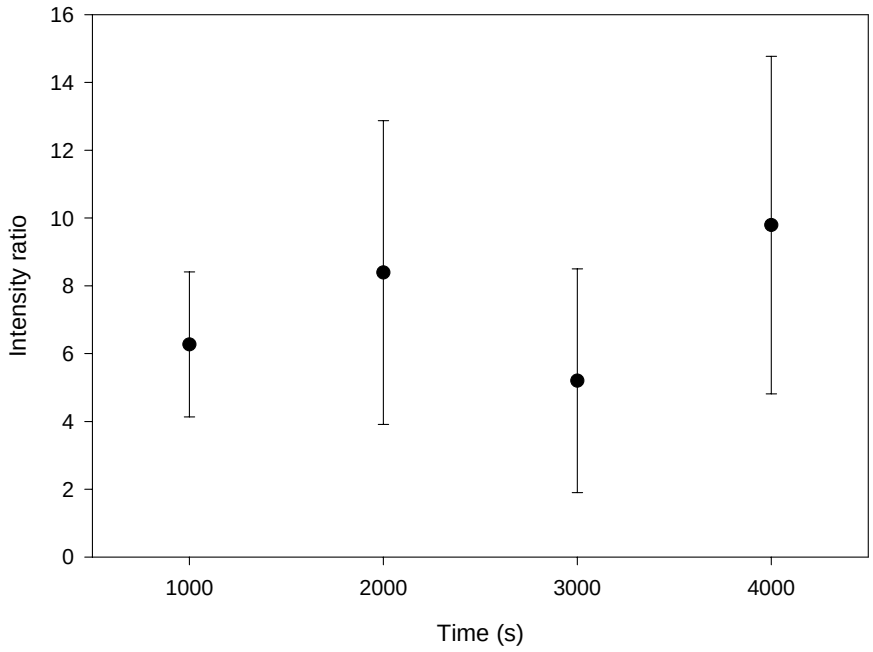

Figure 36: Intensity ratio of 660 cm^{-1} band (indicative of xanthate) to that of the 743 cm^{-1} band as a function of the anodic polarization time. Anodic polarization was carried out at 0.2V (SHE) in a 0.05 M $Na_2B_4O_7$ solution containing 1 x 10^{-3} M potassium ethyl xanthate. Error bands indicate 95% confidence intervals for a single run, with around 5 measurements for each 1000s of polarisation time.

Although the formation of dixanthogen is evident from the results, it has been shown that chemisorption of xanthate or the formation of metal xanthate itself establishes a non-zero contact angle resulting in a hydrophobic surface (Woods *et al.*, 2000). The fact that xanthate could be identified within 120 seconds, indicates that the interaction of the collector with the mineral should yield a hydrophobic surface even after short conditioning time.

Raman spectroscopy elucidated the nature of the reduction reactions of the cathodic leg of the cyclic voltammograms. When, after anodic polarization, the potential of the Pd-Bi-Te was decreased to 0.1V (which is in the region of the higher-potential cathodic peak – see figure 22 – and is below the xanthate-dixanthogen equilibrium potential) the band at 498 cm^{-1} was no longer observed. Figure 37 shows the Raman spectrum observed for a Pd-Bi-Te electrode held at 0.1V (SHE) in a 10^{-3} M KEX

solution at pH of 9.2 (see middle spectrum) after being polarized at 0.2V (SHE) (bottom spectrum). It is important to note that the cathodic peak in the higher potential region is more positive than the xanthate-dixanthogen equilibrium potential. Thus, the cathodic peak (see Figure 28a) in the higher potential region cannot be the result of the reduction of the bulk phase (i.e. dixanthogen) only and may involve the reduction of metal oxides which formed during anodic polarisation (for instance bismuth oxide). When the sample was subsequently held at – 0.2V for extended periods (6000s) the intensity of the 660 cm^{-1} band (xanthate) decreased relative to the 743 cm^{-1} band for the same recording conditions. It hence appears that the cathodic peak in the lower potential region arises from the reduction of the xanthate (either present as a monolayer or metal xanthate) and the dixanthogen.

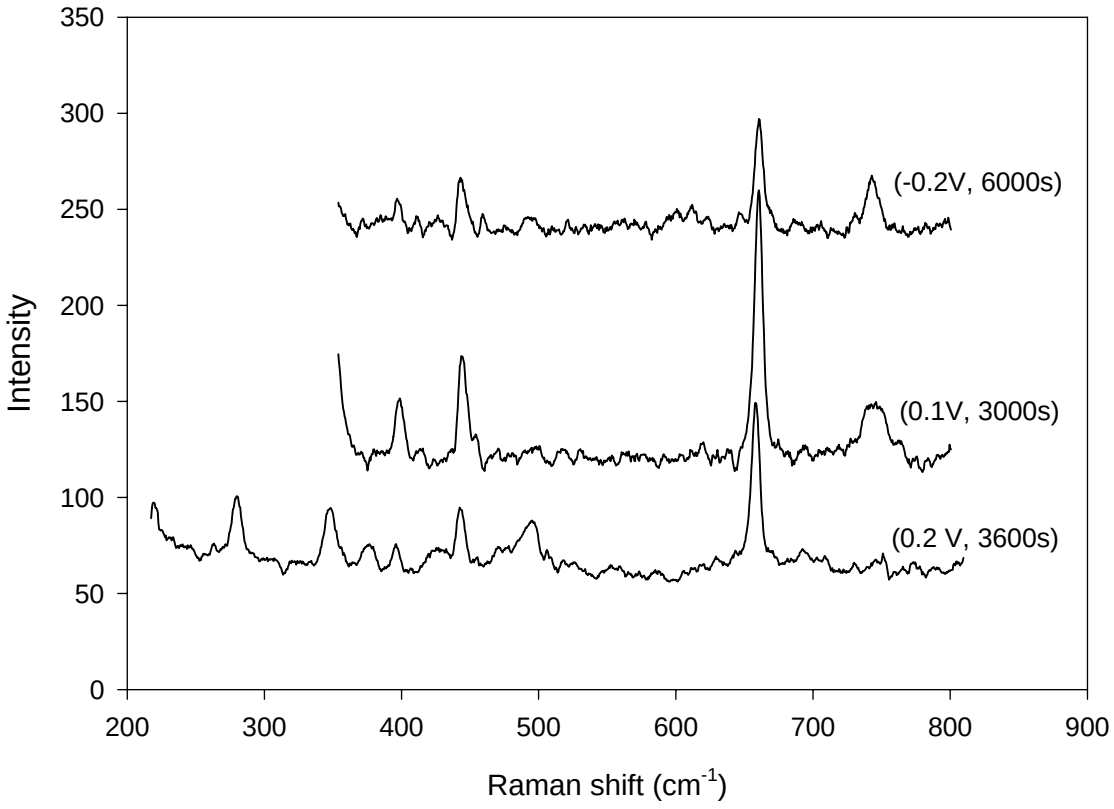

Figure 37: Raman spectra of Pd-Bi-Te electrode polarised at 0.2 V for 3600s, and subsequently at 0.1V and –0.2V (SHE) in 0.05 M $Na_2B_4O_7$ solution containing 10^{-3} M potassium ethyl xanthate. Laser power of 100mW and recording time of 120 seconds.

5.2.3. Oxidation of Pd-Bi-Te

The comparatively weak bands located at 283 cm^{-1}, 350 cm^{-1} and 743 cm^{-1} (see the *in situ* spectrum in Figure 32) could not be related to either ethyl xanthate or diethyl dixanthogen. The band at 743 cm^{-1} shows considerable broadening, perhaps indicative of poor crystallinity of the related phase. The peaks could not be identified from literature data: palladium and tellurium sulphides have strong bands at 401cm^{-1} and between 229-264 cm^{-1}, respectively (van der Maas *et al.*, 1987). No data could be found in relation to bismuth.

Figure 28a shows that a net anodic current arises when the Pd-Bi-Te electrode is polarized at 0.3V in a 0.05 M $Na_2B_4O_7$ containing solution. The absence of xanthate indicates that the anodic current is a result of background processes involving the mineral itself i.e. oxidation of the mineral. The possibility that the 743 cm-1 band originates from a mineral oxidation product was investigated.

The nature and dynamics of this band were investigated by polarizing the Pd-Bi-Te surface at 0.3V in the 0.05 M $Na_2B_4O_7$ solution whilst recording Raman spectra over time (see results in Figure 38). The figure clearly indicates that no marked increases in the intensities of the 743 cm^{-1} bands (shaded in Figure 38) relative to the background could be identified over time. This constancy makes this band a useful point of comparison for the xanthate and dixanthogen bands, as discussed earlier.

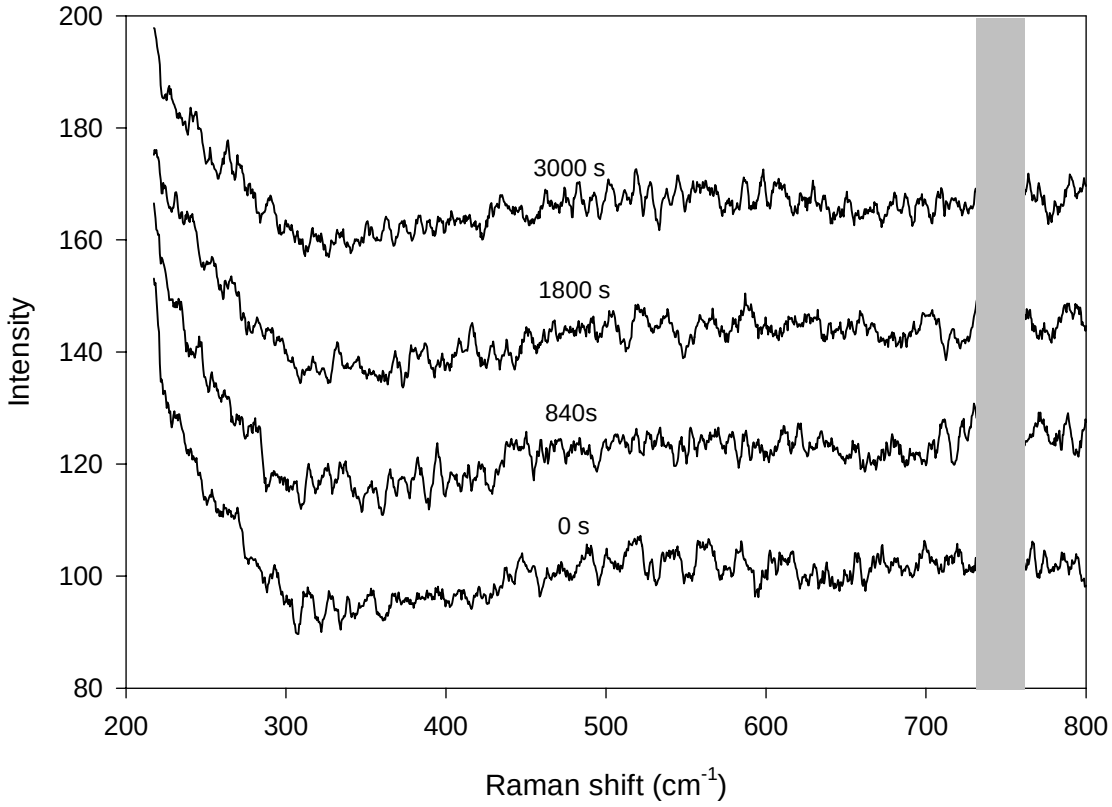

Figure 38: Raman spectra recorded of the surface of the Pd-Bi-Te electrode polarised at 0.3V (SHE) in a 0.05 M $Na_2B_4O_7$ solution containing no xanthate. Laser power rating of 100mW and recording time of 120 seconds. The 743 cm^{-1} band is highlighted.

To test the possible origins of the 743 cm^{-1} band, various pretreatments were applied to the Pd-Bi-Te sample, followed by the measurement of the Raman spectra. In all cases, the sample was first ground and polished (according to the procedure listed in Chapter 4), followed by immersion in the borate buffer solution polarised at 0.3 V (SHE), or drying in a stream of purified argon for 5 minutes (sample was kept in argon during measurements), or exposure to air (10 minutes were allowed for air to diffuse into the cell previously filled with purified argon). The resulting Raman spectra are shown in Figure 39, together with a reference spectrum for a concentrate buffer solution and a spectrum for the Pd-Bi-Te after anodic polarisation [0.3 V (SHE) for one hour in a $1x10^{-3}$ M potassium ethyl xanthate solution]. The spectrum of the concentrated buffer solution was recorded in a glass macro cell hence the peak

between 300 cm^{-1} and 500 cm^{-1} (see $Na_2B_4O_7$ (aq) spectrum in figure 39) reflects the absorbance of the glass.

Figure 39 clearly indicates that the oxidation of the mineral in air causes a band at 743 cm^{-1}, which corresponds to the spectrum measured after anodic oxidation in borate. Exposure of the mineral to purified argon gas did not cause a band to appear at this position, indicating that the band formed in air is a result of the interaction of the laser with the surface in the presence of oxygen. However, the results are somewhat ambiguous: the borate buffer solution does give a peak around 750 cm^{-1} and – as shown later – a peak was also found at this position for sperrylite in borate buffer. It hence cannot be stated with certainty whether the peak originates only from a mineral oxidation product or only the borate buffer. Nevertheless, the consistent height of this peak during polarisation did make this a useful reference band.

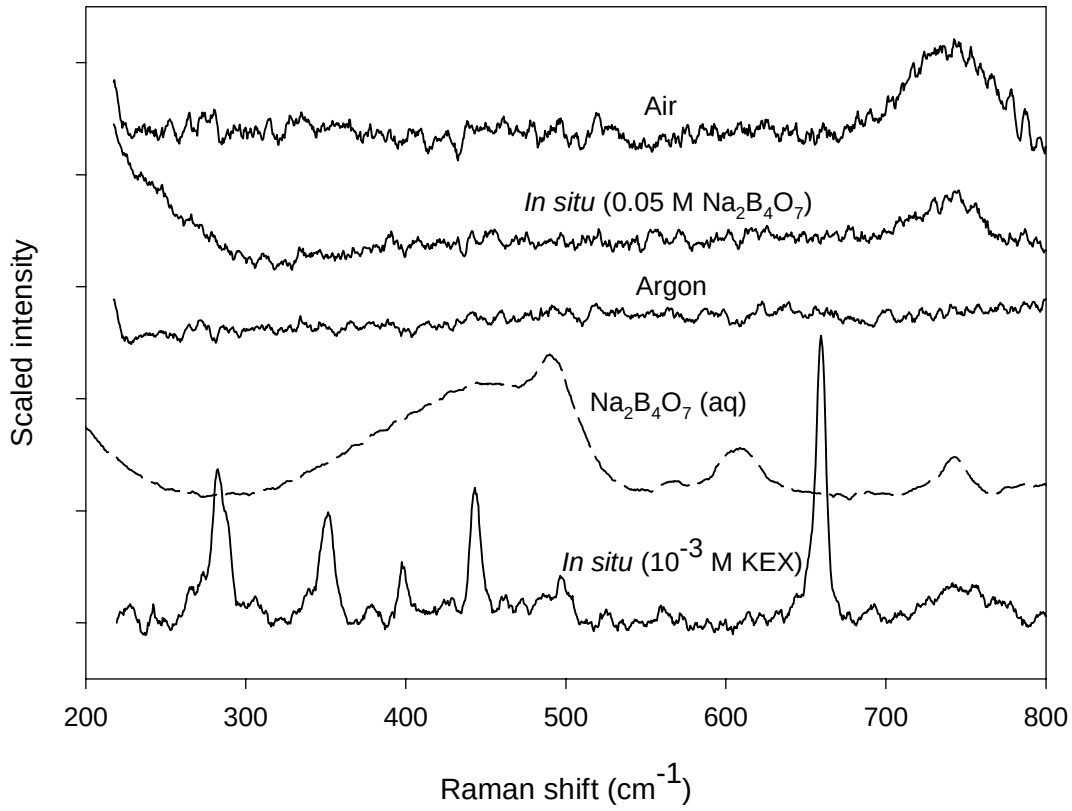

Figure 39: *In situ* Raman spectra recorded of Pd-Bi-Te in the presence of KEX, argon, borate and air, respectively (*In situ* spectrum: Pd-Bi-Te electrode polarised at 0.3 V (SHE) for 3600s in 0.05 M $Na_2B_4O_7$ solution containing 1 x 10^{-3} M potassium ethyl xanthate; $Na_2B_4O_7$ (aq) spectrum: glass macro cell containing saturated borate solution; argon spectrum: sampled dried in purified argon for 5 minutes; *In situ* 0.05 M $Na_2B_4O_7$ spectrum: Pd-Bi-Te electrode polarised at 0.3 V (SHE) for 3600s in a 0.05 M $Na_2B_4O_7$-containing solution; air spectrum: spectrum taken in air). Laser power rating of 100 mW and recording time of 120 seconds.

5.2.4. Results of Raman spectroscopy on $PtAs_2$

Similar Raman measurements were performed with the synthetic sperrylite sample. An *in situ* Raman spectrum from a $PtAs_2$ electrode polarized for 2600s at 0.3V (SHE) in 0.5 molar sodium tetraborate solution containing 1 x 10^{-3} molar potassium ethyl xanthate is shown in Figure 40. Figure 40 also shows the Raman spectra obtained from freshly synthesized potassium ethyl xanthate and diethyl dixanthogen. Table 9 shows the energies of some of the characteristic bands in the Raman spectrum of the $PtAs_2$ measured in the presence of xanthate at 0.3V (SHE) and corresponding bands of synthesized potassium ethyl xanthate and diethyl dixanthogen.

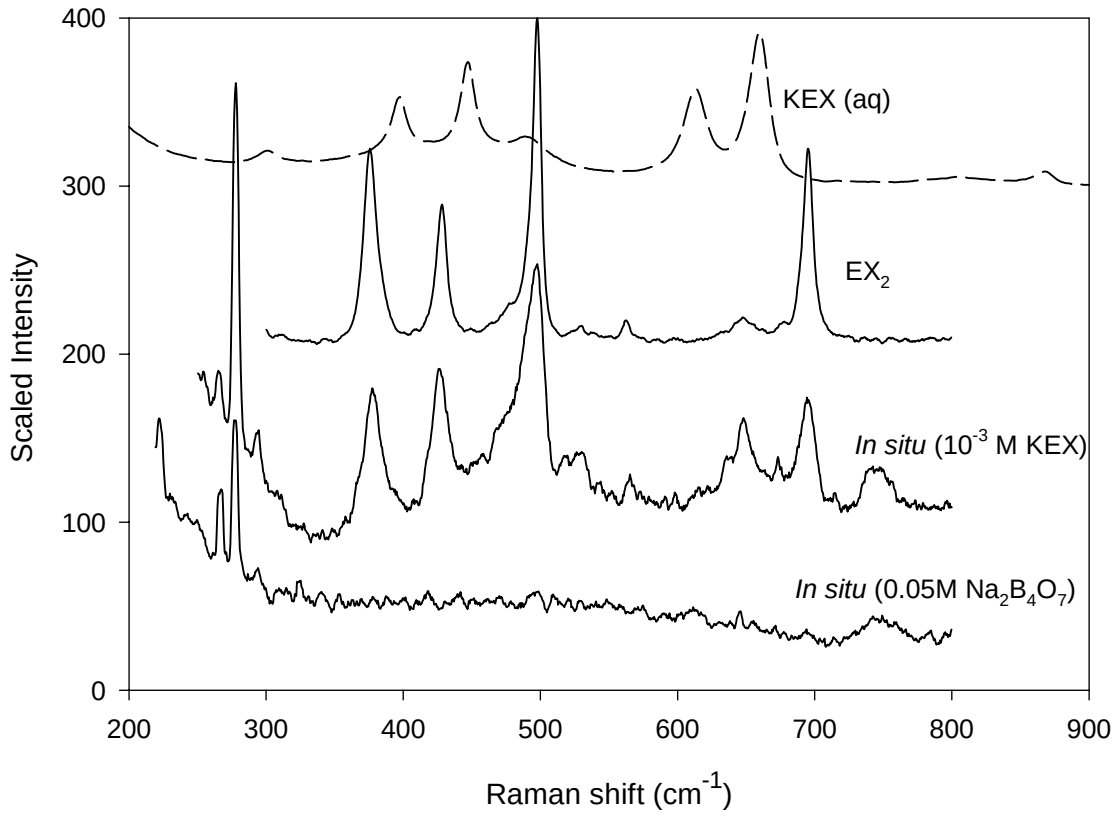

Figure 40: Raman spectra recorded of freshly synthesized potassium ethyl xanthate, diethyl dixanthogen and the *in situ* spectrum of the surface of $PtAs_2$ after polarization at 0.3V (SHE) in a 0.05 M $Na_2B_4O_7$ solution for 2600s in the presence (1 x 10^{-3} M potassium ethyl xanthate) and absence of xanthate. Laser power rating of 100mW and recording time of 120 seconds.

Table 9: Characteristic Raman bands of xanthate compounds and of $PtAs_2$, which was anodically polarised in the presence of ethyl xanthate. Assignment of the bands of the xanthate compounds was based on the work published by Woods *et al.* (1998).

Vibration	KEX (aq)	EX_2 (l)	*In situ* 300 mV
CS_2 antisymmetric stretch	1046	1041	1041
CCOC stretch	864	845	846
CS_2 symmetric stretch *trans*	660	695	695
CS_2 symmetric stretch *gauche*	615	646	647
OCS_2 out of plane *wag*	556	528	527
SS stretch	n.a.	498	498
COC deformation *gauche*	493	473	-
COC deformation *trans*	449	427	427
OCC deformation	399	378	377

n.a. not applicable

The bands located at 278 cm^{-1} and 745 cm^{-1} (see the in situ spectra) could not be related to either ethyl xanthate nor diethyl dixanthogen. The Raman spectrum of pure platinum and arsenic taken in air are also shown in Figure 41. The Pt-Pt bond only shows bands in the region of 180-195 cm^{-1}, in close agreement with published data (van der Maas *et al.*, 1987). The band located at 743 cm^{-1} was found for both electrodes studied (see Figures 32, 34 and 41) and can probably be assigned to the buffer solution, even though the results in Figure 39 indicate an additional contribution from oxidation of the Pd-Bi-Te electrode.

Figure 40 displays a band at 498 cm^{-1}, which demonstrates the presence of dixanthogen on the surface. The anodic peak shown in Figure 30a hence reflects oxidation of xanthate to dixanthogen. In contrast to the spectra observed on the Pd-Bi-Te no clear bands could be found from chemisorbed xanthate on the surface of the mineral. However, the formation of dixanthogen on the surface could be detected after short polarisation times as shown in Figure 41. When compared with Pd-Bi-Te, the kinetics of the formation of dixanthogen is much faster on the $PtAs_2$. The presence of a chemisorbed xanthate layer on sperrylite cannot be ruled out – the layer may

simply be undetected because of poor enhancement of the Raman signal. Although the phenomenon of SERS is not fully understood, it is known that not all substrates facilitate SERS.

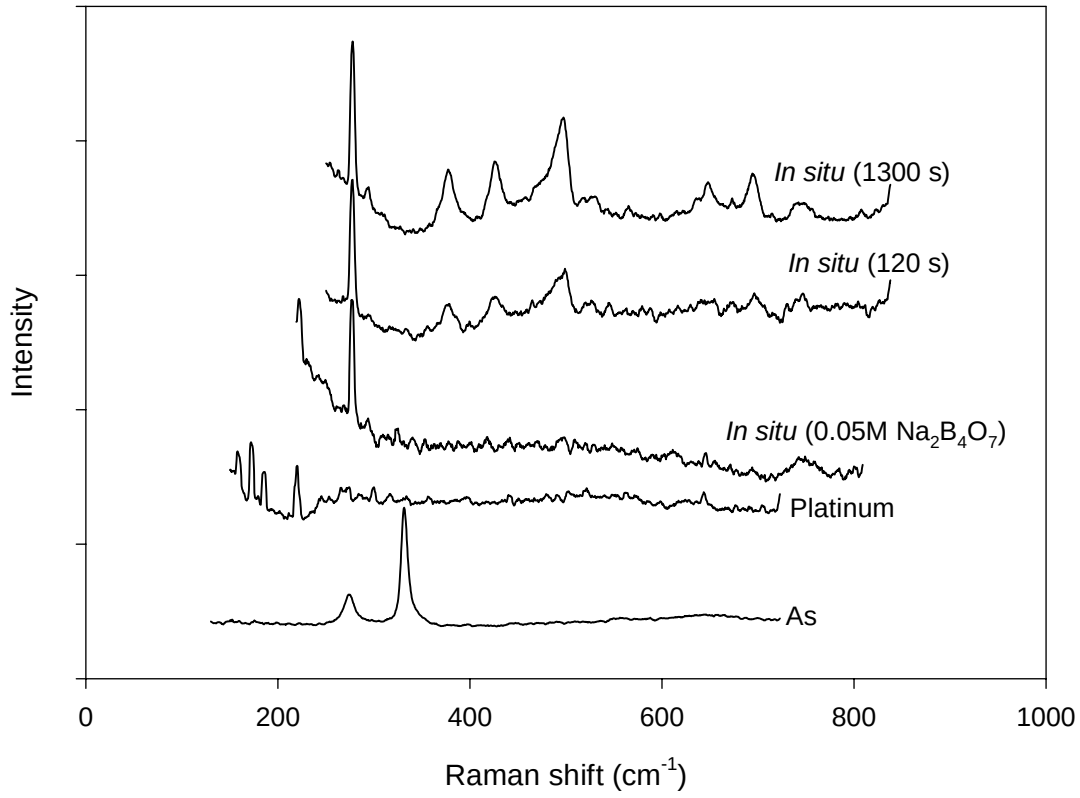

Figure 41: Raman spectra of $PtAs_2$ electrode polarised at 0.3 V (SHE) in 0.05M $Na_2B_4O_7$ solution containing 1 x 10^{-3} M potassium ethyl xanthate for different times (see top two plots). Spectra of $PtAs_2$ in 0.05M $Na_2B_4O_7$ solution (third plot) and of pure platinum and arsenic taken in air (second from bottom and bottom, respectively). Laser power of 100mW and recording time of 120 seconds.

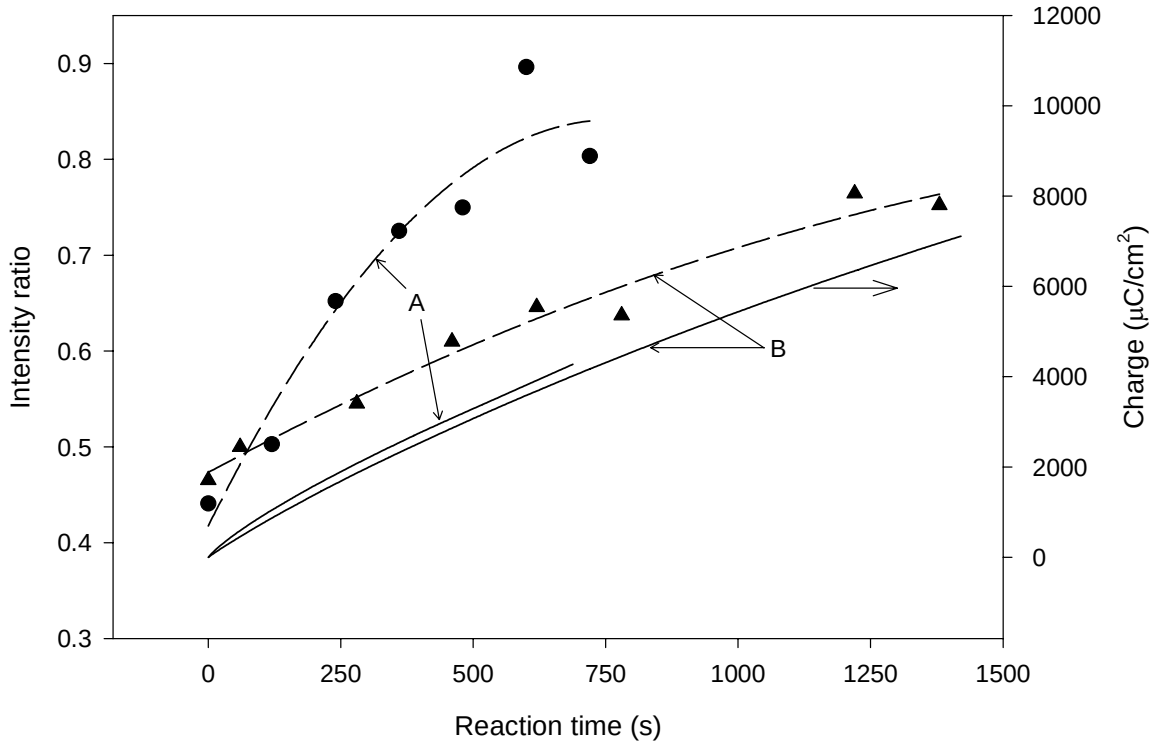

Figure 42: Intensity ratio of 498 cm^{-1} (dixanthogen) band relative to that of the 275 cm^{-1} (sperrylite) band as a function of the anodic polarization time (data points and broken lines). Anodic polarization of sperrylite was carried out at 0.3V (SHE) in a 0.05 M $Na_2B_4O_7$ solution containing 1 x 10^{-3} M potassium ethyl xanthate. The total anodic charge passed during polarization is also shown (full lines). "A" and "B" are data sets from two different sets of measurements.

Figure 42 plots the intensity ratio of the 498 cm^{-1} band (dixanthogen) relative to the 275 cm^{-1} band (sperrylite base-line) and the associated measured anodic charge transfer for two different sets of measurements, A and B, as functions of reaction time. It is unlikely that the conditions for the *in situ* measurements, for example fluid flow patterns over the electrode, were the same for every run, hence the difference in measured anodic current is not surprising. Nevertheless, Figure 42 clearly indicates that larger anodic charges can be related to increased amounts of dixanthogen on the mineral surface.

5.3. Flotation kinetics of Pd-Bi-Te

5.3.1. Introduction

The flotation behaviour of the liberated PGMs is mostly affected by the type of PGM and grain size. The previous sections of this chapter investigated the electrochemically interaction of ethyl xanthate with synthetic Pd-Bi-Te and $PtAs_2$ by employing impedance measurements, voltammetry, Raman spectroscopy and electrochemically controlled contact angle measurements.

To summarise the results for Pd-Bi-Te: Impedance measurements on Pd-Bi-Te which had been anodically polarised in the presence of ethyl xanthate for prolonged times indicated the formation of a continuous surface layer. The mixed (open-circuit) potential of the mineral is more positive than the xanthate-dixanthogen couple, indicating the possibility of forming dixanthogen on the mineral surface. Electrochemically controlled contact angle measurements showed maximum contact angles of 63°, underlining the hydrophobic nature of the surface. Raman spectroscopy confirmed the co-presence of xanthate with dixanthogen on the mineral surface.

From these measurements it is clear that the poor flotation response is not caused by an absence of interaction between the collector and the mineral surface. However, the (static) contact angle measurements do not characterise flotation behaviour directly, because of the kinetic resistance to bubble-particle attachment (Nguyen *et al*., 1998): the induction time (which is extensively used in bubble-particle attachment modelling) better describes the flotation collection. As a result smaller particles show slower flotation rates compared to larger particles. Penberthy *et al.* (1999) found that small liberated platinum-group minerals did float albeit at lower rates. In that work, the average measured particle diameter of the liberated particles in the UG-2 concentrates in the fast- (first-minute concentrate), medium- (second-minute concentrate) and slow-floating concentrates (after 20 minutes) was 8µm, 4µm and 2µm, respectively. The average particle size of the liberated platinum-group minerals found in the rougher tailings of Mimosa Mine was between 3 µm and 4 µm (Van Wouw, 2000). Indeed, the probable reason for loss of the Pd-Bi-Te minerals to tailings is poor flotation kinetics, which in turn may be related to particle size effects.

This study investigated the flotation kinetics with micro-flotation tests. The flotation response of synthetically prepared Pd-Bi-Te minerals was compared with that of typical minerals found in platinum ores, including chalcopyrite (a typical fast-floating mineral) and pyrrhotite (a typical slow-floating mineral). The particle size range was the same in all cases, namely 38 – 106 μm.

5.3.2. Results and discussion

Figure 43 compares the cumulative mass recovery for selected natural minerals with that of synthetic Pd-Bi-Te. The error bars refer to the standard deviation of the triplicate tests.

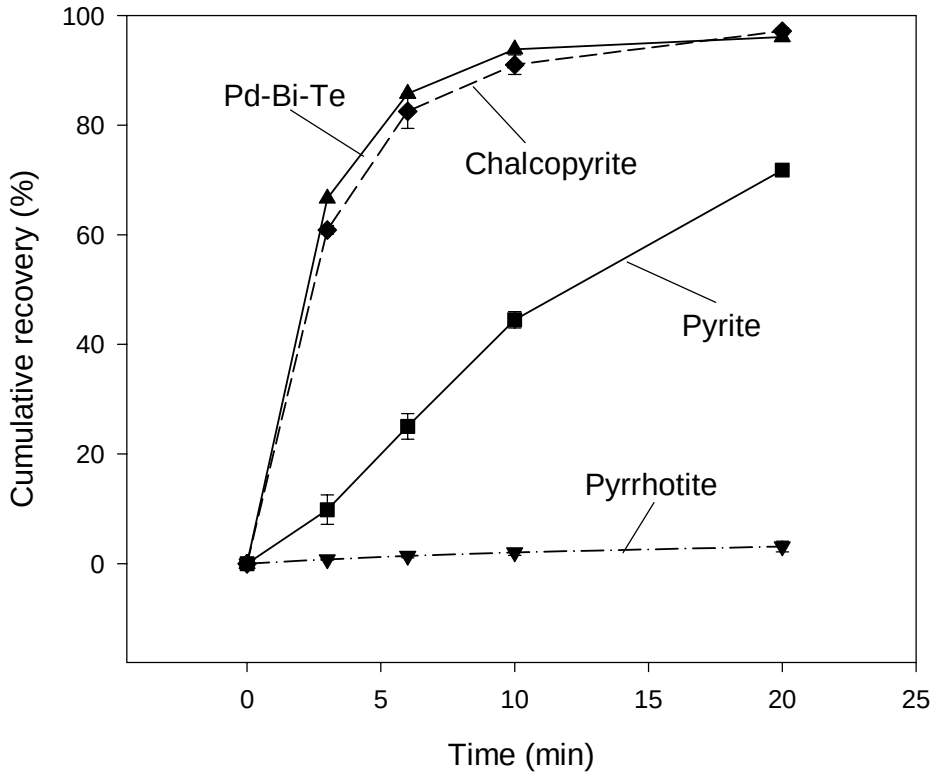

Figure 43: Recovery-time curves during microflotation of selected natural and synthetic minerals in a synthetic solution containing 5×10^{-5} M sodium isobutyl xanthate at pH 9. The particle size range: 38 – 106 μm.

The Figure 43 clearly indicates the poor flotation response of pyrrhotite at pH 9, which corresponds to literature: Senior *et al*. (1994) found that pyrrhotite was rejected at pH 9 in mixtures of pentlandite and pyrrhotite (80g/t potassium ethyl xanthate dosage, without activation). In contrast, Pd-Bi-Te shows a rapid flotation response, similar to that of chalcopyrite, which is known for its fast-floating characteristics. This similarity in the flotation kinetics is reflected by the rate constants which are summarised in Table 10; these rate constants were found by fitting the following Klimpel flotation rate equation to the batch data (Klimpel, 1984):

$$r = R\left\{1 - \left(\frac{1}{kt}\right)\left[1 - \exp(-kt)\right]\right\} \qquad (4)$$

with r = mineral recovery at time t (%)

R = infinite time recovery (%)

k = rate constant (min^{-1})

Table 10. Summary of micro-flotation rate constants of chalcopyrite and Pd-Bi-Te.

	k (min^{-1})	R (%)
Pd-Bi-Te	1.18	97.0
Chalcopyrite	0.92	98.1

In line with the electrochemical and contact-angle measurements, the microflotation work confirms that the Pd-Bi-Te should be recoverable with the regular xanthate collectors.

5.3.3.1. Particle size effects

It is proposed that the small size of the liberated PGMs might be responsible for the poor practical flotation response of these minerals: particle-bubble attachment is influenced by the particle size which affects the collision efficiency (E_c), attachment efficiency (E_a) and particle-bubble stability efficiency (E_s) (Pyke *et al*., 2003). The total collection efficiency of the process is the product of these three sub-processes.

The detailed mathematical description of these sub-processes (Duan *et al*., 2003; Pyke *et al*., 2003) was used here to estimate size effects.

This analytical model (Ralston model) yields flotation rate constants which follow the characteristic trend with particle size, with lower flotation rates for particles at the top and bottom ends of the particle size distribution. The flotation rate constants are largest for particle diameters around 40 μm and 60 μm, for chalcopyrite and quartz respectively (Duan *et al*., 2003; Pyke *et al*., 2003). In contrast, liberated PGM grains are usually much smaller, less than 10 μm in diameter: as stated earlier the average size of the liberated platinum-group minerals in the rougher tailings of Mimosa Mine was between 3μm and 4μm (Van Wouw, 2000).

For the sake of comparison, the rate constants were estimated for a 2.25 dm^3 Rushton cell, as in the previous work (Duan *et al*., 2003; Pyke *et al*., 2003). Tables 11 - 13 summarise the numerical values of the parameters in the calculations. Note in Table 12 that the contact angle on the Pd-Bi-Te is smaller than for chalcopyrite (as listed in table 13); this results in a larger value of the constant A which describes the induction time (Dai *et al*., 1999).

Table 11: Properties of the Rushton cell, as used in the model calculations (Duan *et al*., 2003). V_{cell} is the cell volume, G_{fr} the gas flow rate, v_b the bubble speed, ε the turbulent dissipation energy, and d_b the bubble diameter

V_{cell} (m^3)	G_{fr} (m^3/s)	v_b (m/s)	ε (m^2/s^3)	d_b (m)
2.25×10^{-3}	9.2×10^{-5}	0.2	14	9.70×10^{-4}

Table 12: Ore-related properties as used in model calculations.
Pd-Bi-Te (See text; values of A and B estimated from Dai *et al*., 1999):

A ($s/cm^{-0.6}$)	B (-)	ρ (kg/m^3)	ϕ (°)
0.07	0.6	8474	63

Table 13: Chalcopyrite properties (Duan *et al*.,2003):

A ($s/cm^{-0.6}$)	B (-)	ρ (kg/m^3)	ϕ (°)
0.05	0.6	4100	71

The calculated rate constants, and efficiencies of collision, attachment and stability are given in Figures 44 and 45 as functions of particle size. The lower attachment and stability efficiencies for Pd-Bi-Te result from the higher density and lower contact angle of that mineral. These give generally lower overall collection efficiencies for Pd-Bi-Te, and lower rate constants for particles larger than 20 µm. While this behaviour is not in full agreement with the experimental results in Figure 43 (note that those experimental results are for particles in the range 38-106µm), the rate constants are quite sensitive to the contact angle (and the related induction time constant *A*, which is rather scattered in the available data, Dai *et al*., 1999). The specific contact angle is also dependent on the xanthate species which is present on the mineral surface. For example, for 10 ppm collector concentration, Woods (1974) reported maximum contact angles on platinum of 70^o for diethyl xanthate, and 85^o for dibutyl xanthate. Hence the main conclusion from these predicted rate constants is that these are similar for chalcopyrite and Pd-Bi-Te, and especially so for the small particles, although the rate constant for larger Pd-Bi-Te particles is significant smaller.

This finding is consistent with the slow flotation response of small hydrophobic PGMs as found by Penberthy *et al*. (2000) for UG-2 chromite: small PGMs do float, but at a significantly lower rate.

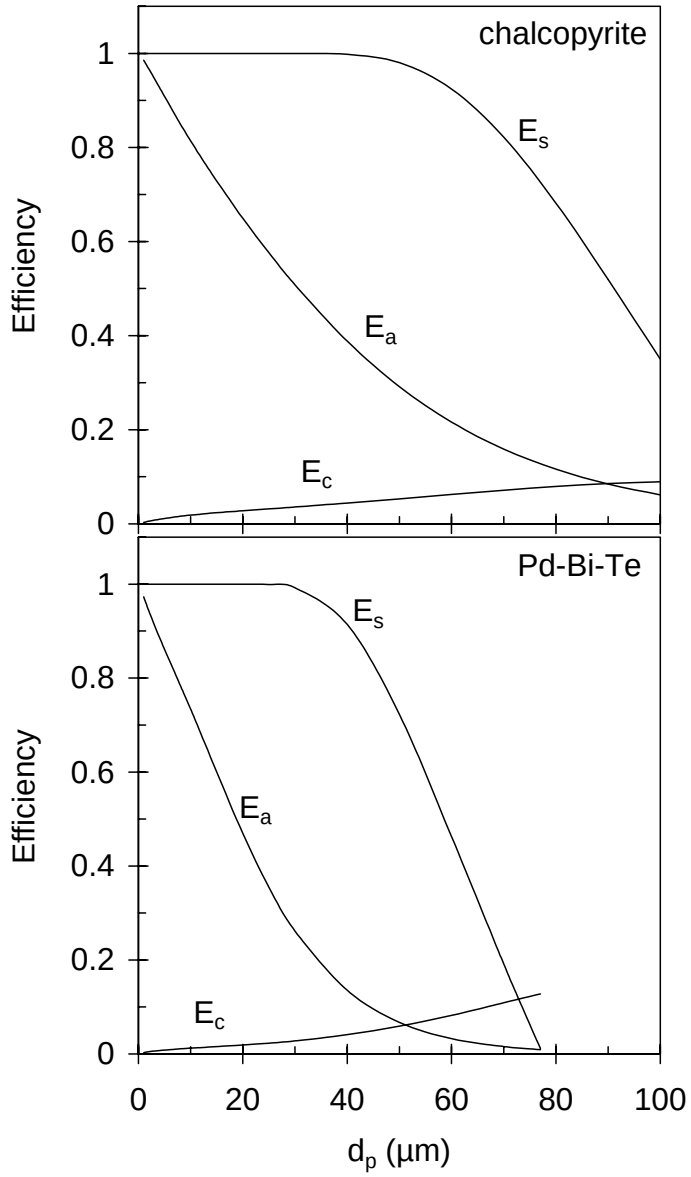

Figure 44. Calculated efficiencies of collision (E_c), attachment (E_a) and stability (E_s) at different particle sizes, for chalcopyrite (upper graph), and Pd-Bi-Te (lower graph).

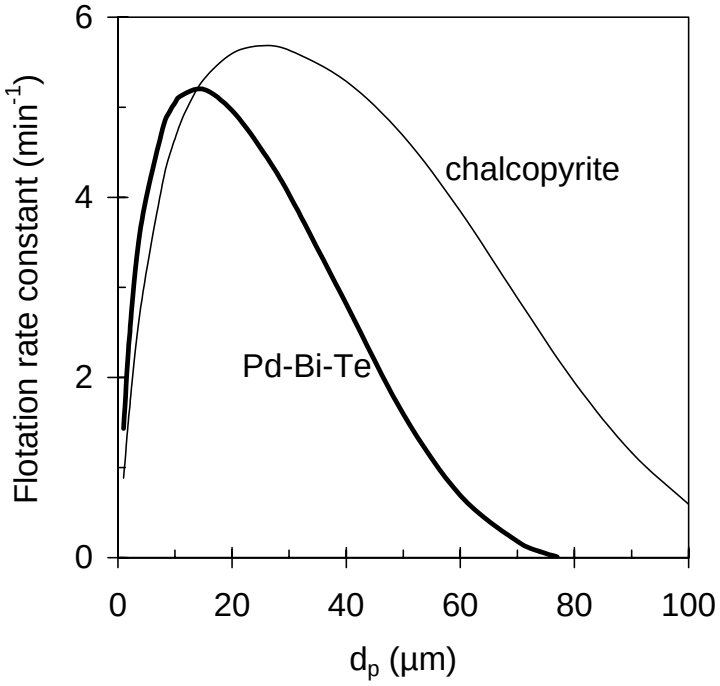

Figure 45. Calculated flotation rate constants at different particle sizes, for chalcopyrite (lighter line), and Pd-Bi-Te (heavier line).